https://doi.org/10.5194/egusphere-2026-2031
Preprint. Discussion started: 14 April 2026

Scale dependence of precipitation structure using Tweedie Poisson–Gamma scaling: an Estonian case study from radar composites and gauges

Yee Chun Tsoi[1], Aarne Männik[1], Sander Rikka[1]

[1]Department of Marine Systems, Tallinn University of Technology, Tallinn, 19086, Estonia

Correspondence to: Yee Chun Tsoi (yeechun.tsoi@taltech.ee)

Abstract. We characterize precipitation structure over Estonia and the surrounding region using Tweedie Poisson–Gamma scaling, with Tweedie power p as a descriptor of aggregation-dependent mean–variance behaviour in zero-inflated, heavily-positive-skewed precipitation. The study extends existing Tweedie precipitation analysis to the joint examination of temporal aggregation, seasonality, spatial variability, and observing-system differences. The analysis uses a 1 km, 5 min radar composite derived from the two Estonian C-band radars together with an OTT Pluvio^2 L gauge network over September 2020 to August 2024. For accumulation lengths from sub-hour to daily windows, p is estimated from block-wise mean and variance statistics using ordinary least squares, with availability filtering to handle missing radar timestamps and matched window sampling for radar–gauge comparison.

Across all data sources, p increases with accumulation length, showing that temporal aggregation changes precipitation mean–variance scaling. Seasonal separation is also clear, with p generally highest in summer and lowest in winter, and winter showing the strongest increase with accumulation. Spatially, the all-year radar fields show strong scale dependence but only weak geographical contrasts at fixed accumulation length, whereas seasonal maps show clearer heterogeneity at longer windows. Radar-based p at station locations is generally higher than gauge-based estimates, and the magnitude and spread of the differences depend on accumulation length and gauge temporal resolution. These results show that p should not be used as a fixed precipitation parameter transferable across durations, seasons, space, or products. Instead, it provides a scale-aware benchmark for evaluating precipitation consistency in generated, corrected, or forecast products, such as quantitative precipitation estimation, downscaling, and nowcasting.

1 Introduction

Radar composites and rain gauges provide the primary description of precipitation and support applications such as flood warning, hydrological design, and short-range forecast verification (Krajewski and Smith, 2002; Berne and Krajewski, 2013). These data sources resolve a wide range of systems, from individual convective cells to stratiform precipitation bands, but their practical use depends on how precipitation occurrence and amounts behave when aggregated from minutes to hours and days. For example, short-range precipitation nowcasting relies heavily on radar-based fields at fine time steps, whereas many

https://doi.org/10.5194/egusphere-2026-2031
Preprint. Discussion started: 14 April 2026

hydrological applications and verification emphasize longer accumulations and multi-duration consistency (Prudden et al., 2020; Langousis and Veneziano, 2007). A statistical description that links behaviour across accumulation lengths and observing systems is therefore useful for interpreting precipitation consistently across time scales.

Rainfall statistics are commonly described using a two-component framework that treats occurrence and amount separately. Let $W_t \in \{0,1\}$ denote the wet–dry indicator and $A_t \geq 0$ denote the precipitation accumulation over interval t. A Markov chain is often used for the discrete occurrence sequence, for example a first-order two-state model where the wet probability depends only on the previous state $W_{t-1} = i$:

$$P(W_t = 1|W_{t-1} = i) = p_{i1},\ where\ i \in \{0,1\}. \quad (1)$$

A continuous distribution is then fitted to amounts on wet intervals, with the Gamma distribution being a common choice:

$$A_t|(W_t = 1) \sim Gamma(k, \theta),\ A_t|(W_t = 0) = 0. \quad (2)$$

This Markov–Gamma framework, originated from early work by Gabriel and Neumann (1962) and later developments for time series (Chin, 1977; Small and Morgan, 1986), has been widely used for stochastic simulation and downscaling in hydrology and climatology. Over the past decades, the basic chain has been extended to non-homogeneous and hidden Markov models (Rajagopalan et al., 1996; Sansom and Thompson, 2001). On the amount side, Gamma models have also been extended with mixed exponentials and other heavy-tailed distributions (Chapman, 1998; Menabde and Sivapalan, 2000), while Martinez-Villalobos and Neelin (2019) recently provided physical arguments for why Gamma-like distributions emerge across climate conditions and averaging times. Yet, most approaches still retain a split between discrete occurrence and continuous amounts, meaning that any summary of variability must combine two separate models or use a multivariate approach. This makes it difficult to compare behaviour consistently across accumulation lengths and data sources, and to extend the framework to high-resolution radar–gauge composites.

An alternative approach is to model precipitation with the Tweedie family, which provides a single mean–variance relationship for zero-inflated, positively skewed totals. In a Tweedie generalized linear model (GLM), the total precipitation amounts Y_t over a given interval has mean μ_t and variance

$$Var(Y_t) = \phi \mu_t^p, \quad (3)$$

where $\phi > 0$ is a dispersion parameter and p is the Tweedie power. For $1 < p < 2$, the Tweedie distribution has a compound Poisson–Gamma representation,

$$Y_t = \sum_{i=1}^{N_t} X_{t,i}, \quad (4)$$

where $N_t \sim Poisson(\lambda_t)$ is a latent number of events and the contributions $X_{t,i}$ follow a Gamma distribution (Hasan and Dunn, 2010). When $N_t = 0$, the total is exactly zero, and when $N_t > 0$, the sum of Gamma contributions gives a continuous, positively skewed amount. While both Markov–Gamma and Tweedie frameworks are consistent with intermittent precipitation and Gamma-like positive amounts, they are typically used for different purposes. Markov–Gamma is commonly used as a time-series model at a fixed base time step to describe wet–dry persistence and wet-interval amount in many stochastic weather generators and downscaling approaches (Richardson, 1981; Wilks, 1999). In contrast, the Tweedie Poisson–Gamma

https://doi.org/10.5194/egusphere-2026-2031
Preprint. Discussion started: 14 April 2026

representation is used as a marginal model for accumulation totals over a chosen interval, providing a direct mean–variance scaling through the power p without modelling wet–dry persistence. This makes it convenient to compare precipitation behaviour consistently across accumulation lengths, seasons, spatial locations, and observing within a single framework.

Previous studies show that Poisson–Gamma models reproduce key precipitation features across accumulation lengths and data sources, which provide a practical GLM framework for analysing scaling and zero inflation (Hasan and Dunn, 2010; Svensson et al., 2017; Hunt, 2025). However, these studies usually focus on a relatively fixed context, such as one accumulation period, an average across seasons, a limited set of locations, or a single data source. For example, Hasan and Dunn (2010) analysed monthly rainfall using the Tweedie distribution in Australia, while Hasan et al. (2019) further compared such behaviour across multiple temporal scales. Later, Rydén (2025) examined monthly precipitation from Swedish gauges and related the estimated Tweedie index to seasonal and geographical differences. Other related studies have considered mean–variance scaling or the choice of Tweedie power in different observational settings and applications (Svensson et al., 2017; Hunt, 2025). While these studies show that Tweedie-based precipitation modelling is useful across a range of climates and data sources, they do not provide a comprehensive view of how the Tweedie power varies simultaneously with temporal aggregation, season, spatial location, and observing system over a high-resolution radar composite domain.

This question is equivalently relevant in the eastern Baltic Sea region, where precipitation reflects a combination of maritime and continental influences, land–sea contrasts, and seasonal differences in precipitation mechanisms. Estonia and the surrounding areas are affected by frequent mid-latitude cyclones and frontal systems throughout the year, while warm-season precipitation is more often influenced by stronger convection and occasional heavy-rain events associated with southern cyclones and other low-pressure systems (Post et al., 2002; Jaagus et al., 2010; Mändla et al., 2014). Spatial contrasts are further introduced by coastline geometry, exposure to the Baltic Sea and Gulf of Finland, and upland terrain toward the southern and eastern part of the Baltic states near Latvia and western Russia (Jaagus et al., 2010; Remm et al., 2011). These geographical features make the region a useful example for examining how precipitation structure changes with scale, season, location, and data source.

In this paper, we apply Tweedie Poisson–Gamma scaling to a 4-year radar composite and rain gauges over Estonia and the surrounding composite domain. The aim is to introduce and evaluate a scale-aware framework for characterizing precipitation behaviour in space and time using a high-resolution radar–gauge dataset, rather than to establish a long-term climatology. We first estimate the Tweedie power p for radar pixels and gauges across a range of accumulation lengths and seasons, and examine how p varies with temporal aggregation, season, and observing system. We then map p to identify spatial patterns across the radar composite domain and assess its agreement between radar composites and gauges. In this way, the study extends existing Tweedie precipitation work and provides a new and unexplored perspective of how Tweedie power can be used to characterize precipitation across space, time, and observing systems. These results are expected to inform the evaluation of precipitation statistics in radar products, nowcasting systems, and other high-resolution earth system models.

https://doi.org/10.5194/egusphere-2026-2031
Preprint. Discussion started: 14 April 2026

2 Data

2.1 Radar composite

In this study, we use observations from the two Vaisala dual-polarimetric Doppler C-band weather radars in Estonia, located at Harku and Sürgavere, each with a maximum range of 250 km. Standard filtering is applied to the reflectivity fields from 11 elevation angles to remove non-meteorological echoes, after which the original polar-coordinate observations are interpolated to a common Cartesian grid and converted to a Pseudo-CAPPI at 1000 m above mean sea level. The reflectivity is then converted to a precipitation-rate estimate using an empirical Z–R relationship that has been used in prior studies with Estonian radars (Voormansik et al., 2021; Cremonini et al., 2023):

$$Z = 300R^{1.5}, \quad (5)$$

where Z is the radar reflectivity (mm^6 m^{-3}) and R is the precipitation rate (mm h^{-1}). The resulting composite is defined on a rectangular grid with 1 km spacing and size 603 × 554, which covers Estonia and encloses the 250 km ranges of both radars (Fig. 1). The analysis grid extends beyond Estonia and includes parts of surrounding countries and the Baltic Sea. Grid cells outside the instrument ranges are treated as missing values. The temporal resolution is 5 min, and the study period spans September 2020 to August 2024.

2.2 Rain gauge network

Estonia is equipped with a network of OTT Pluvio^2 L weighing precipitation gauges. For this study, we use 26 stations with 1 h accumulations available, of which 25 also provide 10 min accumulations. All selected gauges lie within the radar composite domain and represent both coastal and inland settings (Fig. 1). These data are obtained from the Estonian Weather Service and are used directly without further processing. The 1 h series is not identical to hourly sums formed from the 10 min data, and they are therefore treated as separate gauge products in the subsequent analyses. This distinction is also reflected in the slightly different Tweedie power behaviour shown later in the results. Both gauge products are restricted to the same four-year window as the radar composite for consistency.

https://doi.org/10.5194/egusphere-2026-2031
Preprint. Discussion started: 14 April 2026

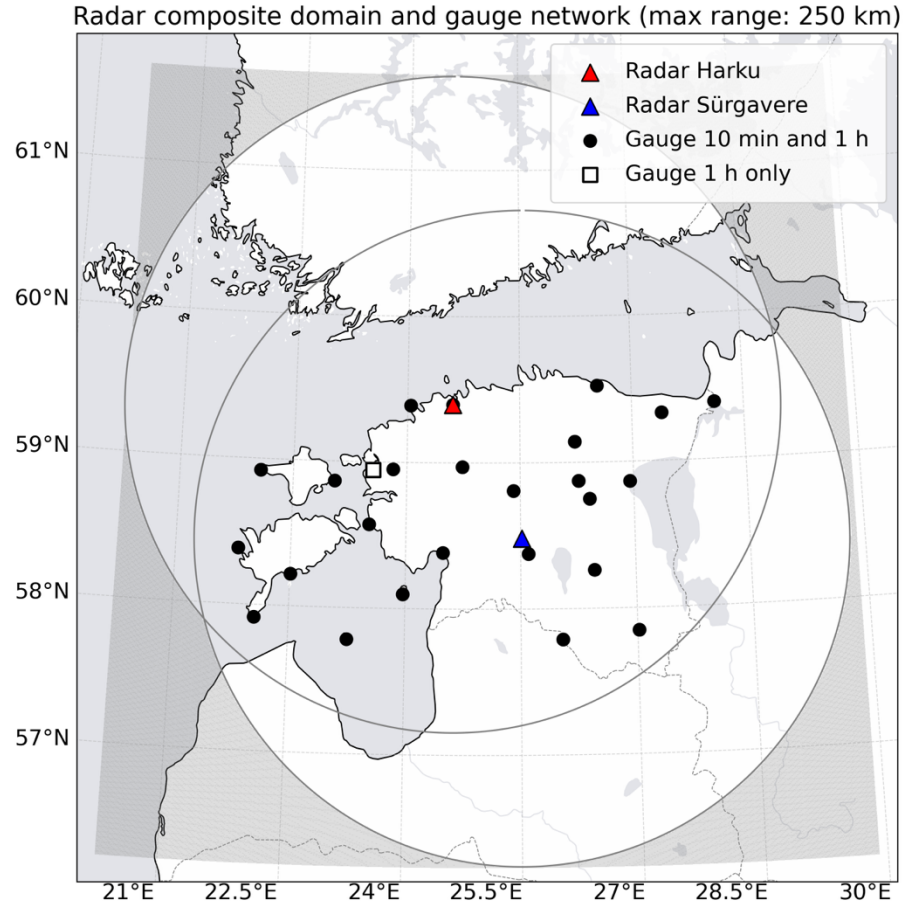

Figure 1: Domain of the composite radar product and observation network used in this study. The shaded area shows the spatial domain of the analysis grid, and the circles denote the coverage ranges of the radars located at Harku and Sürgavere, marked by coloured triangles. Rain gauges with both 10 min and 1 h measurements are shown by filled circles, while the station with 10 min measurements only is shown with an open square.

3 Methods

3.1 Tweedie power estimation

To characterize how precipitation variability changes with temporal aggregation, we use the Tweedie mean–variance scaling of accumulated precipitation Y over an accumulation length τ. From Eq. (3), the scaling can be written as

$$\log Var(Y) = \log \phi + p \log \mu, \tag{6}$$

where μ is the mean, $\phi > 0$ is a dispersion parameter, and p is the Tweedie power. For $1 < p < 2$, this corresponds to a compound Poisson–Gamma process with a point mass at zero and a continuous positive tail. We estimate p for the accumulation lengths listed in Table 1, only when the accumulation lengths are available for the corresponding data product. For each accumulation length τ, the time series is split into non-overlapping windows of length τ, which are then grouped into

https://doi.org/10.5194/egusphere-2026-2031
Preprint. Discussion started: 14 April 2026

non-overlapping multi-day blocks of length L. The block length is selected separately for each τ to provide adequate within-block samples for stable mean–variance regression.

Accumulation period τ	Block length L (days)
5 min	5
30 min	10
1 h	10
6 h	15
24 h	15

Table 1: Block length L in days used for mean–variance estimation of Tweedie power p at each accumulation period τ.

Furthermore, missing 5 min time steps in the radar series are handled by two availability thresholds. A window is considered valid only if the fraction of frames within that window exceeds a per-window threshold of 0.98, and a block is retained only if the fraction of valid windows within that block exceeds a block-level threshold of 0.90. These thresholds are used to balance data size against availability, rather than being tuned or optimized. Gauge windows are required to be complete at their native temporal resolution. Each retained block is then assigned to a season, winter (DJF), spring (MAM), summer (JJA), and autumn (SON), according to its midpoint timestamp.

For each retained block b, we compute the block-level mean μ_b and variance s_b^2 across window totals within the block. Tweedie power p is then estimated by ordinary least squares (OLS) as the slope of the mean–variance relationship across blocks, by fitting

$$\log s_b^2 = \log \phi + p \log \mu_b + \varepsilon_b, \quad (7)$$

using only blocks where $\mu_b > 0$ and $s_b^2 > 0$. The fit is performed separately for each accumulation length and each season, producing per-pixel p estimates for radar and per-station p estimates for gauges. We use the standard error from OLS fit as an uncertainty measure.

Additionally, we extended the estimated p curves for gauge series below their shortest analysed accumulations by assuming a linear relationship in $\log \tau$ beyond the available accumulation points. These extrapolations are included only as an exploration of the gauge behaviour toward shorter accumulation lengths and do not suggest strictly linear behaviour. To further illustrate how p values relate to the distribution of accumulation precipitation, we also examine one representative station at 24 h accumulation using point-wise distributional plots. At this station, empirical histograms are compared with fitted Gamma and Tweedie distributions and between seasons to illustrate how differences in p are reflected in the spread and shape of the corresponding distributions.

3.2 Radar–gauge comparison

Rain gauges are compared with the radar composite by extracting the radar accumulation from the grid cell containing each station. To ensure consistent comparisons under missing time steps, we construct matched non-overlapping windows by

https://doi.org/10.5194/egusphere-2026-2031
Preprint. Discussion started: 14 April 2026

retaining only those windows that satisfy the availability filtering defined in Sect. 3.1 so that both estimates are based on identical temporal samples. Tweedie power is then estimated separately for the radar-at-station and gauge series using the same non-overlapping block construction and mean–variance regression as in Sect. 3.1.

For each station, season, and accumulation length, the radar–gauge difference is defined as the difference between the radar-at-station and gauge Tweedie powers. These station-wise differences are then summarized across the stations using the median and interquartile range (IQR). The median is used to represent the systematic difference between radar and gauge estimates, while the interquartile range is used to describe the spread of the station-wise differences in a way that is less sensitive to individual outlying station than using full range or standard deviation. This provides a summary of both the central tendency and the between-station variability of the radar–gauge differences.

4 Results

4.1 Tweedie power overview

Across all-year samples (Fig. 2), the estimated Tweedie power p increases with accumulation length for every data product, rising from around 1.5–1.7 at sub-hour accumulations to approximately 1.6–1.9 at 6–24 h. This indicates that, as precipitation is aggregated over longer windows, the variance increases more rapidly with the mean. In physical terms, longer accumulations are less dominated by isolated short wet spells and increasingly reflect the combined contribution of multiple precipitation episodes within a window. Across the common accumulation lengths, the three products show a consistent ordering, with the radar composite giving the highest p, followed by the 10 min gauge series, while the 1 h gauge series is lowest. This difference likely reflects differences in temporal sampling and representativeness of products, rather than different precipitation regimes. Finer temporal sampling retains sharper wet–dry transitions and short-scale variability, whereas coarser sampling smooths those transitions and reduces heterogeneity at shorter accumulation lengths. In addition, radar values represent grid-cell averages while gauges represent point measurements, which can further shift the Tweedie power between products.

Fig. 2 also includes extrapolations of the p curves for the gauge products below their shortest analysed accumulation lengths. They are obtained by assuming a linear relationship with $\log \tau$ from the available accumulation points. However, the radar curve itself does not suggest a strictly linear relationship over the shortest accumulation range, particularly between 5 and 30 min, while the expanding shaded areas indicate increasing uncertainties from both OLS fitting and extrapolation. The extrapolated segments therefore provide additional context for how the gauge series might behave toward shorter accumulation lengths, rather than estimations for the actual short-scale scaling.

https://doi.org/10.5194/egusphere-2026-2031
Preprint. Discussion started: 14 April 2026

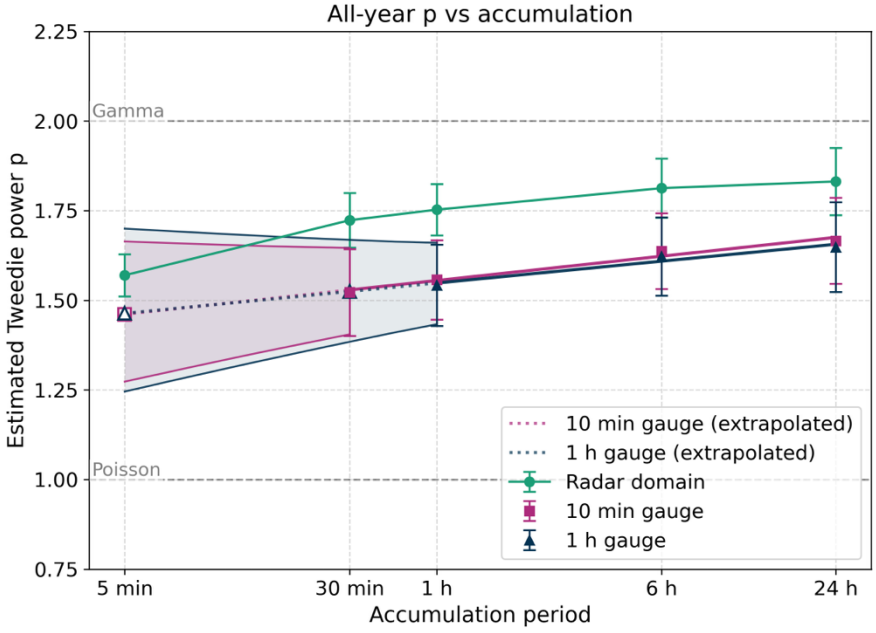

Figure 2: All-year estimates of Tweedie power p versus accumulation length for the radar composite and gauge series at 10 min and 1 h resolution, on a logarithmic x-axis. Markers show estimates at each accumulation length and error bars indicate standard errors from OLS fitting. Dashed horizontal lines indicate the Poisson ($p = 1$) and Gamma ($p = 2$) limits. For the gauge products, the dashed lines below the shortest analysed accumulation lengths are extrapolated by assuming a linear relationship in $\log \tau$ from the available accumulation points, and those error bars combine uncertainties from both OLS fitting and extrapolation.

Seasonality is also clear in both the radar composite and the gauge series (Fig. 3a–c). Across all data products, p is highest in JJA, the summer season, and lowest in DJF, the winter season. This ordering can be explained by warm-season precipitation being more influenced by convective and localized variability, while the cold season is more dominated by synoptic systems with relatively persistent precipitation structures (Alber et al., 2015; Voormansik et al., 2021; Olsson et al., 2022). On the other hand, the seasonal separation depends on accumulation length. In the radar estimates, DJF shows the steepest increase in p with accumulation, while JJA varies less with aggregation (Fig. 3a). This suggests that temporal aggregation alters the structure of wet–dry transitions more strongly in winter than in summer. The same behaviour is also visible in the gauge series (Fig. 3b–c), indicating that the seasonal ordering and its dependence on accumulation length are not specific to a single product.

https://doi.org/10.5194/egusphere-2026-2031
Preprint. Discussion started: 14 April 2026

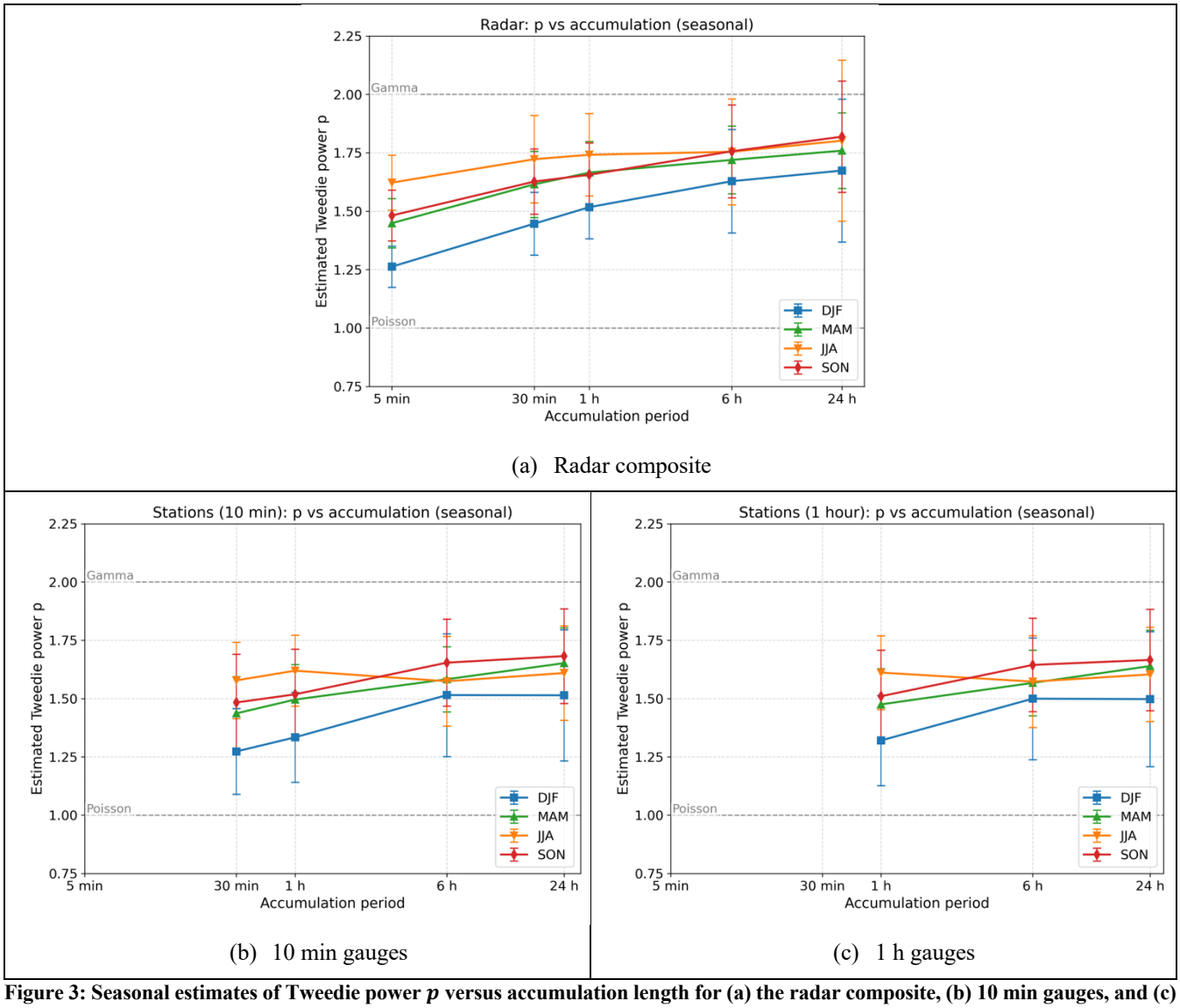

Figure 3: Seasonal estimates of Tweedie power p versus accumulation length for (a) the radar composite, (b) 10 min gauges, and (c) 1 h gauges, on a logarithmic x-axis. Colours denote DJF (winter), MAM (spring), JJA (summer), and SON (autumn). Markers show estimates at each accumulation period and error bars indicate standard errors from OLS fitting. Dashed horizontal lines indicate the Poisson ($p = 1$) and Gamma ($p = 2$) limits.

4.2 Point-wise distributions

To illustrate how p values relate to the shape of precipitation distributions, we use Kuusiku as a representative station and focus on 24 h accumulation (Fig. 4 and 5). This station is used because it lies between the two radar sites and is less influenced by topography, while the 24 h accumulation is chosen because the distributions are less dominated by zero than at shorter accumulation lengths and therefore easier to read visually. In both figures, the x-axis is logarithmic, and the histograms include all 24 h totals, including zeros. In contrast, the Gamma curve in Fig. 4 is fitted to positive totals only, while the Tweedie curve

https://doi.org/10.5194/egusphere-2026-2031
Preprint. Discussion started: 14 April 2026

is also shown only for the positive range, using the fitted p value with the corresponding distributional parameters. Both curves are therefore shown as reference densities for the positive range and do not match the histogram bar heights directly.

Fig. 4 compares the all-year 24 h radar distribution at Kuusiku with fitted Gamma and Tweedie curves. Both curves reproduce the positively skewed behaviour of the distribution and remain fairly similar over the positive range shown. The main theoretical difference is that the Tweedie model can accommodate zero values, even though the plotted Tweedie curve here shows only its positive part. The figure therefore focuses on illustrating how the fitted p value relates to the overall positive-range distributional shape, rather than a direct goodness-of-fit comparison.

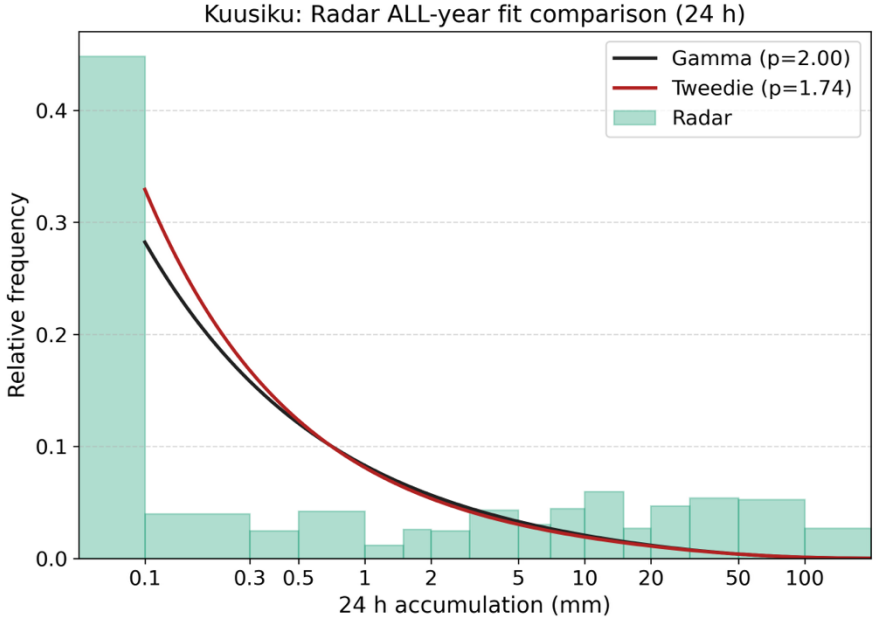

Figure 4: All-year 24 h radar precipitation distribution at Kuusiku, together with fitted Gamma and Tweedie curves, on a logarithmic x-axis. The histogram includes all totals, with the leftmost bar collecting totals below 0.1 mm, including zeros. The fitted curves are plotted only for positive totals and are shown as references for the overall positive-range distributional shape and do not match the histogram bar heights directly.

Fig. 5 compares the 24 h radar distributions at Kuusiku in DJF and JJA. The JJA distribution is more broadly spread, with both a larger proportion of zeros to very low totals and a heavier upper tail, while the DJF distribution is more concentrated in the middle range. This shows that the seasonal difference is not only a matter of more frequent high precipitation totals in summer, but also a broader spread across the lower and upper tails. At this station, the Tweedie power p is slightly higher in JJA than in DJF, which is consistent with the domain-wise seasonal differences shown in Sect 4.1 and the broader warm-season distribution seen in the histogram. A radar–gauge comparison at the same station is also shown in Fig. A1, illustrating the local cross-product differences in the 24 h accumulation distribution shapes.

https://doi.org/10.5194/egusphere-2026-2031
Preprint. Discussion started: 14 April 2026

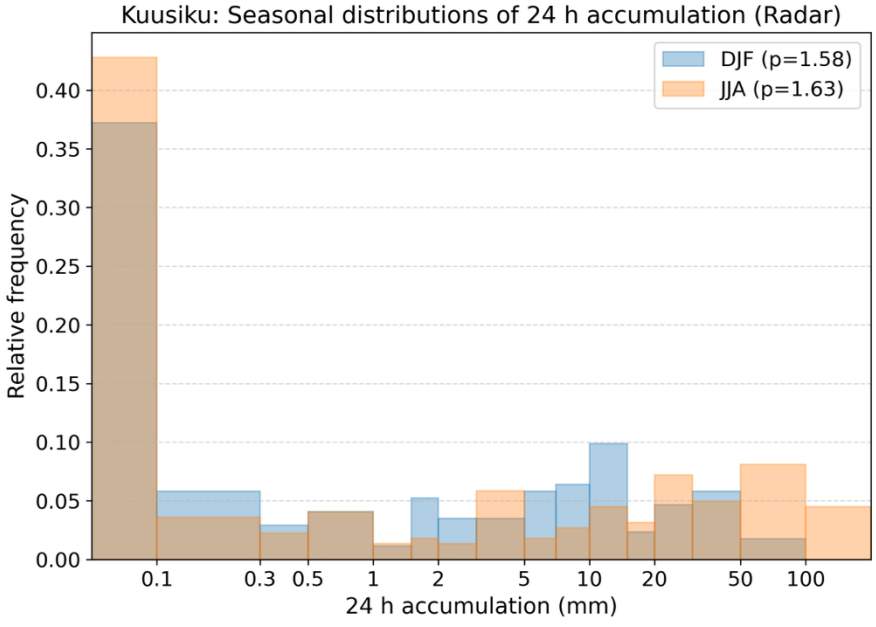

Figure 5: Seasonal 24 h radar precipitation distributions at Kuusiku for DJF and JJA, on a logarithmic x-axis. The histograms include all totals, with the leftmost bar collecting totals below 0.1 mm, including zeros, to show how the empirical spread changes between seasons at station level.

4.3 Spatial patterns in Tweedie power

4.3.1 All-year radar spatial structure

The all-year radar p maps (Fig. 6a–e) show a clear dependence on temporal aggregation, with p increasing systematically with accumulation length, as already seen in Sect. 4.1. However, at any fixed accumulation length, spatial contrasts across the domain remain small compared with the domain-wide shift with aggregation. The all-year means do not show a strong land-sea separation or a clear directional separation. Across all accumulation lengths, the maps also show narrow azimuthal streaks radiating from the radar sites and, at shorter accumulation lengths, ring-like structures. These non-meteorological artefacts still appear despite standard filtering and quality control applied to the composite (Sect. 2.1). They can reflect a combination of ground clutter, anomalous propagation, attenuation effects, and occasional signal interference. We acknowledge their presence but do not interpret them as precipitation structure.

Beyond these artefacts, the remaining spatial variation is relatively weak but broadly persistent across accumulation lengths. Values of p tend to be slightly lower in the central part of the domain near the radar sites and slightly higher toward outer parts of the domain, most notably toward the southeastern inland area near Latvia and Russia, the southern Finland area, and the western coastal area near Saaremaa. This contrast may partly reflect radar sampling effects, including beam geometry and attenuation, which can project onto mean–variance scaling in accumulation precipitation. At longer accumulation lengths, the spatial organization becomes a little clearer, despite gradients in the all-year means remain subtle.

https://doi.org/10.5194/egusphere-2026-2031
Preprint. Discussion started: 14 April 2026

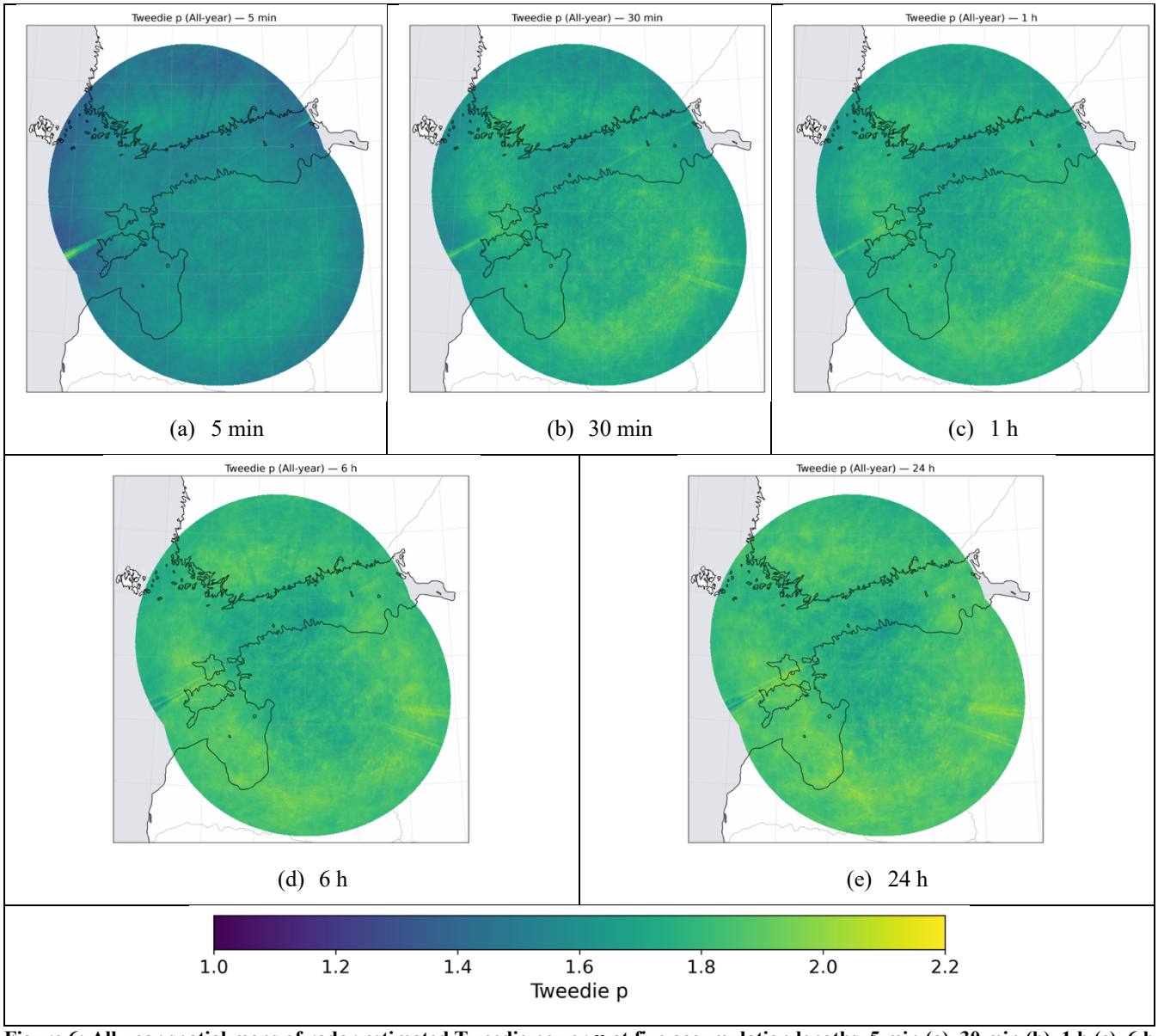

Figure 6: All-year spatial maps of radar-estimated Tweedie power *p* at five accumulation lengths, 5 min (a), 30 min (b), 1 h (c), 6 h (d), and 24 h (e).

4.3.2 Seasonal radar spatial structure

To examine how spatial patterns in Tweedie power *p* vary with season, we focus on 6 h and 24 h accumulations (Fig. 7a–h). These longer accumulation lengths are selected because they show clearer spatial contrasts, while the shorter-accumulation maps are relatively uniform and more affected by non-meteorological artefacts. With longer windows, repeated seasonal regimes stand out more clearly because individual short-lived features contribute less to the seasonal mean. This also aligns

https://doi.org/10.5194/egusphere-2026-2031
Preprint. Discussion started: 14 April 2026

with the seasonal spread maps (Fig. B1), which show that the spatial heterogeneity of radar-estimated p becomes clearer as accumulation length increases.

In DJF (Fig. 7a–b), p is lowest overall compared with other seasons, as seen in Sect. 4.1, and the fields are relatively smooth. At both 6 h and 24 h, lower p extends over much of inland Estonia and across the Gulf of Finland region toward southern Finland, while higher p appears toward the western edge over the open Baltic, specifically at 24 h. The inland structure can be explained by winter precipitation being more frequently associated with synoptic-scale systems and frontal stratiform precipitation, which tend to produce longer wet spells and fewer wet–dry transitions. By contrast, sea-effect precipitation may occur over the open Baltic during cold-air outbreaks, where relatively warm water enhances surface heat and moisture fluxes and favour shallow convection with sharper wet–dry transitions (Olsson et al., 2020; Virman et al., 2025). Similar setups may also occur over the Gulf of Finland, but precipitation there can also take the form of larger-scale, shore-parallel, quasi-stationary snow bands under specific conditions, which would favour longer wet spells than more cellular convection (Savijärvi, 2012; Mazon et al., 2015). In addition, more frequent ice cover in the Gulf of Finland than over the Baltic Proper could suppress sea-effect intermittency in the seasonal mean (Singh et al., 2025). The ring-like patterns around the radars also appear unique to DJF and are likely to reflect range-dependent discontinuities between elevation angles in Pseudo-CAPPI construction, with their visibility potentially enhanced in winter by weaker echoes and mixed-phase precipitation (Tabary, 2007; Seo et al., 2011).

In MAM (Fig. 7c–d), the maps are the most homogeneous among the four seasons. Spatial contrasts remain weak, with slightly lower p near southwestern Finland and relatively higher values toward the south near Latvia. These weak signals may be associated with spring as a transition season in which sea-surface conditions remain relatively cool while land-surface heating is still developing, limiting the contrast between organized stratiform and stronger convective precipitation.

On the other hand, JJA (Fig. 7e–f) shows the highest overall p among seasons, again consistent with Sect. 4.1, with the strongest spatial heterogeneity. The land–sea contrast is amplified at 24 h, with higher p over inland parts of the domain, most notably toward Latvia and western Russia and along the northern edge near Finland, while lower values remain over the Gulf regions and much of Estonia. This pattern fits warm-season precipitation being more strongly influenced by localized convection over land, where short-lived cells and lines sharpen wet–dry transitions and increase event-to event variability (Voormansik et al., 2021). In contrast, precipitation over water is more often associated with broader and longer-lived stratiform or frontal structures. The inland enhancement also aligns with the upland topography in the southern and eastern part of the domain, which has been linked to regional precipitation contrasts and may strengthen inland spatial signals in the seasonal mean (Jaagus et al., 2010; Remm et al., 2011). Furthermore, southern cyclones provide an additional context for the enhanced p toward the southeast at longer accumulation lengths, since they contribute a non-negligible fraction of precipitation and thunderstorms in the region (Mändla et al., 2012; Mändla et al., 2014). Occasional slow-moving or quasi-stationary systems over western Russia may further affect the 24 h pattern by changing how multiple precipitation episodes are integrated within longer windows (Röthlisberger et al., 2022).

https://doi.org/10.5194/egusphere-2026-2031
Preprint. Discussion started: 14 April 2026

In SON (Fig. 7g–h), *p* remains relatively high and heterogeneous compared with DJF and MAM, with clearer organization at 24 h than at 6 h. Higher *p* appears in coastal areas, including southwestern Estonia near Saaremaa and the Gulf of Riga, and parts of southern Finland, while inland regions remain closer to the seasonal mean. This pattern is potentially due to autumn precipitation being more influenced by frequent cyclonic activity over the Baltic region together with coastal enhancement sharpening wet–dry transitions near exposed shorelines (Jaagus et al., 2008).

Season \ Accumulation	6 h	24 h
DJF	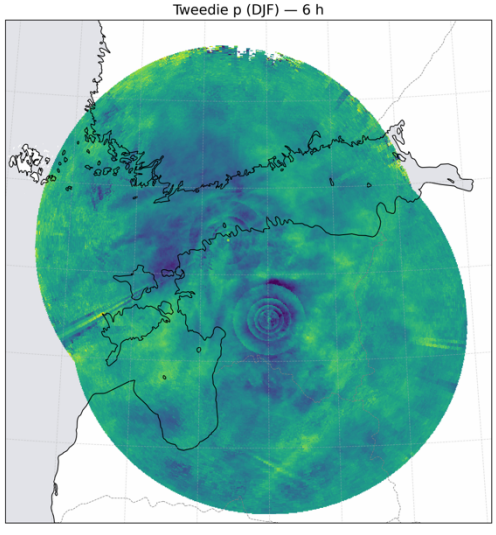 (a)	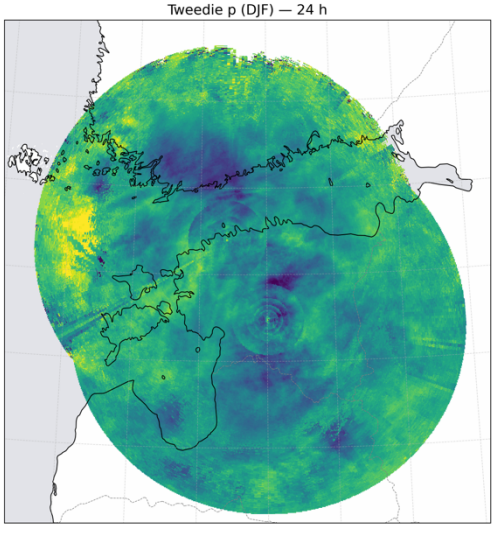 (b)
MAM	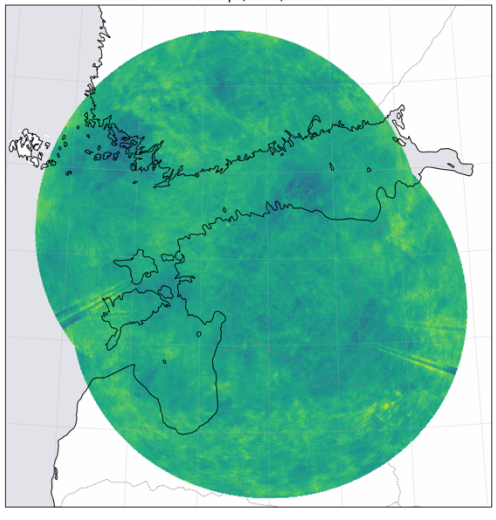 (c)	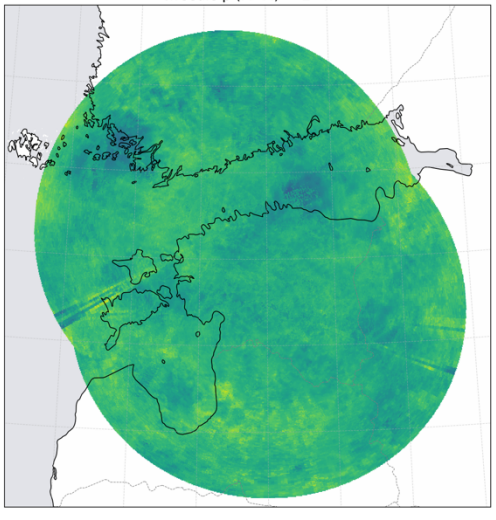 (d)

https://doi.org/10.5194/egusphere-2026-2031
Preprint. Discussion started: 14 April 2026

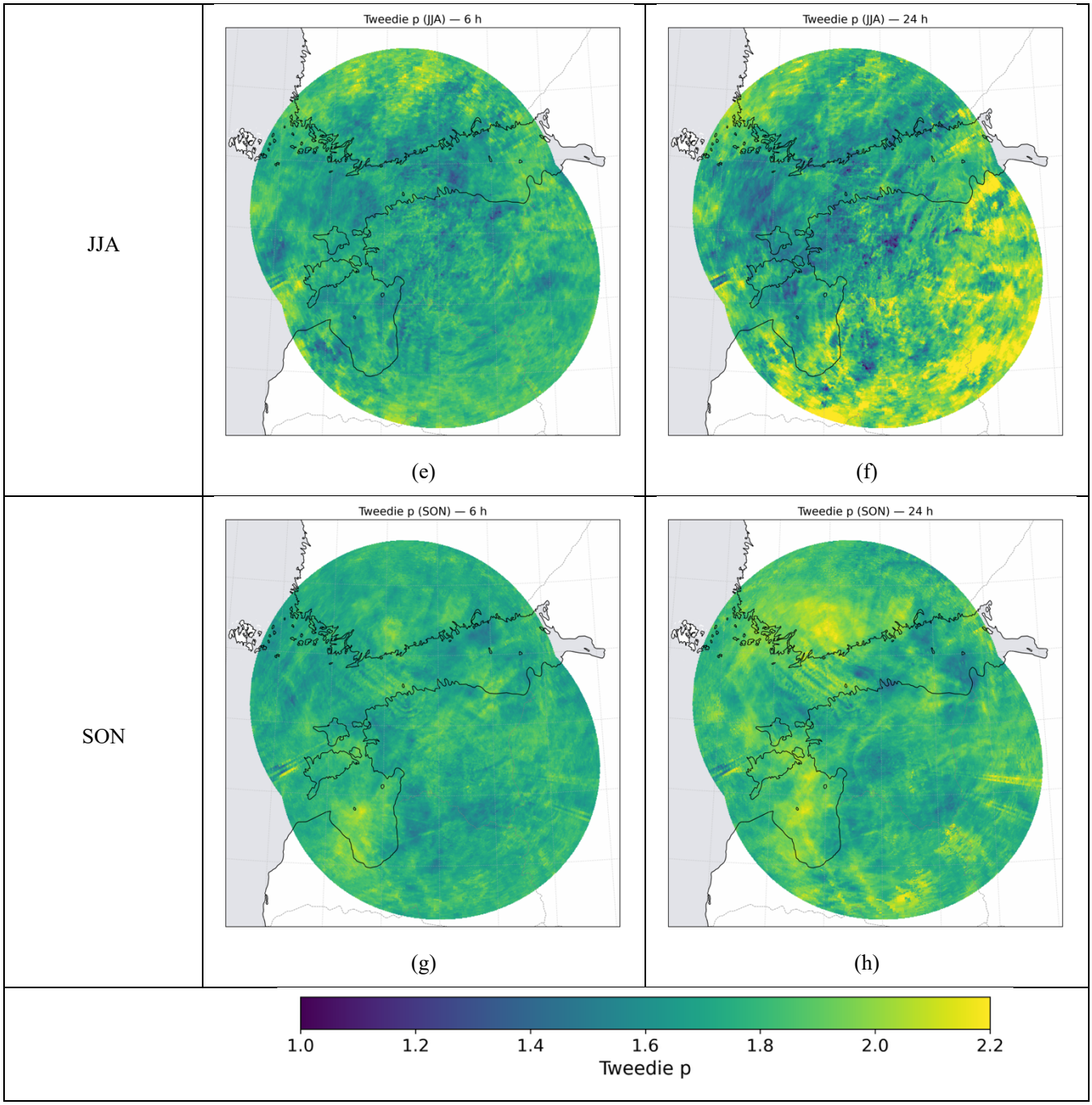

Figure 7: Seasonal spatial patterns of radar-estimated Tweedie power p for 6 h (left column) and 24 h (right column) accumulations. Rows show DJF (a–b), MAM (c–d), JJA (e–f), and SON (g–h).

https://doi.org/10.5194/egusphere-2026-2031
Preprint. Discussion started: 14 April 2026

4.4 Radar–gauge agreement

Tables 2 and 3 summarize the radar–gauge difference $\Delta p = p_{radar} - p_{gauge}$ across stations for the 1 h and 10 min gauge series, respectively, using the median and IQR. Across all seasons and accumulation lengths, the median Δp remains positive for both gauge products, indicating that p estimated from the radar composite at station locations is higher than that from the gauges, consistent with the domain-averaged comparison in Sect. 4.1. In most cases, the median Δp decreases with accumulation length, suggesting that the radar-gauge difference weakens with aggregation. However, the decrease is not strictly monotone in every season, and in some cases, the smallest median difference occurs at 6 h rather than 24 h. Seasonally, MAM shows the largest median Δp and the most consistent decrease with accumulation length, whereas JJA has the smallest median Δp at shorter accumulation lengths.

On the other hand, the spread of Δp across stations, quantified by the IQR, shows a stronger seasonal influence than simple scale dependence. In JJA and SON, the IQR is relatively small at short accumulation lengths but tends to increase toward longer ones. This suggests that warm-season radar–gauge differences become more heterogeneous across stations as aggregation increases, which links to the stronger spatial heterogeneity seen at longer windows described in Sect. 4.3.2. By contrast, DJF shows the largest IQR across stations at all accumulation lengths, while MAM shows more moderate IQR and weaker changes with aggregation, suggesting that cold-season radar–gauge differences are more location-dependent and less controlled by accumulation length alone.

At common accumulation lengths, the 1 h gauge product shows a larger median Δp than the 10 min product for every all-year and seasonal estimate, indicating a larger radar–gauge difference for the coarser gauge series. In contrast, the spread of Δp is less systematically ordered between the gauge series, with the IQR varying by season and accumulation length. We also inspected seasonal and multi-scale maps of Δp (Fig. C1), but spatial patterns are not consistent across scales or seasons. The dominant behaviour is therefore captured more clearly by the station-wise shifts than any map-scale pattern.

Season \ Accumulation	1 h	6 h	24 h
ALL	0.255 (0.085)	0.183 (0.071)	0.157 (0.096)
DJF	0.155 (0.279)	0.147 (0.207)	0.175 (0.321)
MAM	0.206 (0.143)	0.124 (0.112)	0.096 (0.153)
JJA	0.087 (0.115)	0.062 (0.130)	0.097 (0.211)
SON	0.187 (0.106)	0.113 (0.151)	0.146 (0.178)

Table 2: Median and interquartile range of $\Delta p = p_{radar} - p_{gauge}$ across stations for the 1 h gauge series. p_{radar} is computed with radar values taken from the grid cells containing the stations.

Season \ Accumulation	30 min	1 h	6 h	24 h
ALL	0.281 (0.100)	0.238 (0.101)	0.170 (0.082)	0.146 (0.083)

https://doi.org/10.5194/egusphere-2026-2031
Preprint. Discussion started: 14 April 2026

DJF	0.147 (0.249)	0.142 (0.249)	0.136 (0.242)	0.129 (0.361)
MAM	0.249 (0.141)	0.200 (0.149)	0.107 (0.102)	0.084 (0.169)
JJA	0.100 (0.074)	0.070 (0.107)	0.051 (0.128)	0.093 (0.243)
SON	0.200 (0.105)	0.184 (0.084)	0.107 (0.117)	0.119 (0.231)

Table 3: Median and interquartile range of $\Delta p = p_{radar} - p_{gauge}$ across stations for the 10 min gauge series. p_{radar} is computed with radar values taken from the grid cells containing the stations.

5 Discussion

5.1 Summary

Across the radar composite and gauge records, the Tweedie power p varies with both accumulation length and season. In all-year estimates, p increases from sub-hour to daily accumulations for every data source, indicating that temporal aggregation changes the mean–variance scaling of accumulated precipitation. Seasonal separation is also clear across accumulation lengths, with p generally highest in summer and lowest in winter, while winter shows the strongest increase with accumulation length. Spatially, the all-year radar p fields show clear scale dependence but weak geographical contrasts at fixed accumulation lengths, whereas the seasonal maps show stronger heterogeneity at longer accumulation lengths, where regional organization becomes more distinguishable. In the radar–gauge comparison, radar estimates at station locations are generally higher than gauge-based estimates across seasons and accumulation lengths, while the station-to-station spread of the cross-source difference depends on season, accumulation length, and gauge temporal resolution. The point-wise distributional examples further show that differences in p are reflected in differences in the spread and shape of precipitation at station level. Overall, these results show that accumulation length and season strongly control the Tweedie power over the study domain, while spatial structure and cross-product differences remain important for interpreting how p varies within and between products.

5.2 Implications

By characterizing precipitation behaviour through Tweedie power p across accumulation length, season, and space, this study provides a scale-aware target that can constrain precipitation modelling. This is especially relevant in methods that generate precipitation across durations from inferred statistics. For example, in stochastic rainfall simulation, parameters are often calibrated at one temporal resolution and then carried across durations, even though aggregation changes the underlying variability structure. Reproducing precipitation statistics consistently across temporal scales therefore remains challenging and has motivated composite stochastic modelling strategies (Paschalis et al., 2014). The observed increase of p with accumulation length and its seasonality provide an empirical target for checking whether generated series preserve realistic aggregation-dependent variability rather than seasonal means or distributions. The same issue appears in rainfall disaggregation, whose purpose is to derive finer-scale series from coarser observations while preserving variability and extremes, including spatio-temporal disaggregation and Bartlett–Lewis schemes (Wheater et al., 2005; Segond et al., 2006; Kossieris et al., 2018). The

https://doi.org/10.5194/egusphere-2026-2031
Preprint. Discussion started: 14 April 2026

demonstrated benefits of enhanced temporal-resolution precipitation inputs, in terms of model performance and hydrological response, further emphasize the important of preserving a realistic scaling structure when moving between durations (Ficchì et al., 2016; Huang et al., 2019).

The framework is useful in a similar way when observations are corrected, merged, or derived into products. Instead of checking whether a model can generate realistic variability, the issue becomes whether processing has altered the variability structure once the product is used across durations. The radar–gauge difference in p, and its dependence on season, accumulation length, and gauge temporal resolution, link directly to quantitative precipitation estimation (QPE) workflows that combine or correct products. Radar–gauge adjustment and merging methods are widely used for hydrology, and their performance depends on precipitation regime, scale, and the observing networks available (Goudenhoofdt and Delobbe, 2009; Ochoa-Rodriguez et al., 2019; Sokol et al., 2021). Our results suggest that cross-product differences are not limited to means or quantiles but also extend to mean–variance scaling and it change with aggregation. As a result, a product aligned at one duration may still distort the duration dependence needed for downstream applications, which has been seen in quantile-based bias correction (Maraun, 2013; Cannon et al., 2015). The same issue also appears in extreme-value analysis, where radar QPE are commonly used across durations to derive return periods and intensity–duration–frequency relationships (Marra and Morin, 2015). In that context, p can be used as a consistency check before combining products, applying correction, or fitting extreme-value relationships.

The Tweedie power p can also be viewed as a realism benchmark for whether precipitation fields produced by numerical or data-driven models capture realistic intermittency, aggregation dependence, seasonal structure, and spatial contrast. For example, in statistical downscaling, the question is not simply whether the finer-scale target field remains realistic in local distributional properties but also how variability is expressed across scales, such as dry-day frequency and dry-spell duration (Maraun et al., 2010; Tabari et al., 2021). For regional and climate model output, the same framework offers a way to assess whether simulated precipitation fields reproduce realistic scale- and season-dependent variability, rather than appearing plausible only in broad climatological summaries. This matters for regions such as the Nordic–Baltic area, where observed rainfall extremes are geographically heterogeneous and strongly affected by local variability at sub-daily scales (Olsson et al., 2022). On the other hand, in nowcasting and short-range forecasting, where radar-based methods are commonly evaluated across multiple spatial and temporal aggregations, forecast skill depends strongly on scale and precipitation regime (Germann and Zawadzki, 2002; Bowler et al., 2006; Imhoff et al., 2020). The scale-aware Tweedie power in this study can not only assess whether a nowcast preserves the observed variability structure of precipitation, but also whether that structure evolves realistically with lead time. This is relevant to a known problem in precipitation forecasting, where outputs can become overly smooth and under-represent intense precipitation over time scales (Prudden et al., 2020; Ravuri et al., 2021; Cambier van Nooten et al., 2023). The same framework can also motivate distribution-aware training objectives for machine-learning models. For example, Tweedie-deviance-based losses can outperform squared-error baselines for semi-continuous precipitation in a way that depends on aggregation (Hunt, 2025). In that sense, p is useful both as an evaluation benchmark

https://doi.org/10.5194/egusphere-2026-2031
Preprint. Discussion started: 14 April 2026

and as a guide for designing models, especially when high-resolution precipitation predictions are increasing used for downstream applications such as early warning, flood forecasting, and related impact chains (Imhoff et al., 2022).

5.3 Limitations

Radar composites are affected by measurement and processing uncertainties that vary in space, season, and precipitation intensity. These include ground clutter, anomalous propagation, attenuation during heavy precipitation, beam-height effects that change with range, and sensitivity to calibration and filtering choices. Gauges also introduce additional limitations related to point representativeness and temporal resolution that influence short-accumulation statistics. In addition, the analysis is based on a four-year archive with non-negligible missing timestamps, especially in the radar record. This required availability thresholds when forming accumulations and window totals, which adds sampling uncertainty to the estimated p values, as reflected by the fitting standard errors, particularly for longer accumulation lengths and seasonal subsets with fewer effective samples. The present results should therefore be read as a characterization of precipitation structure over a relatively short archive rather than as a long-term climatological study.

Moreover, Tweedie power p highlights when and where precipitation structure differs, but it is not uniquely tied to specific physical mechanisms. For example, similar p values may reflect different combinations of event frequency, duration, and intensity, while observing-system biases may project differently under different conditions. This means that the current framework can identify systematic contrasts in aggregation-dependent variability but cannot by itself fully explain their physical causes, without relating the patterns to other factors such as broader meteorological regimes and climatological context. Potential extensions include repeating the same framework on a longer and more complete archive and comparing alternative products, once they are available. These would also help clarify how much of inferred variability structure depends on data source or processing choices.

6 Conclusions

This study demonstrates a practical way to describe precipitation structure from radar composites and gauges within a single Tweedie framework. The main conclusion is that one particular value of p characterizes precipitation occurrence and amounts in general, but it also changes with accumulation length, season, space, and data source. It should therefore not be treated as a fixed parameter in precipitation modelling that can be transferred without care, but as a consistency check on whether precipitation behaves realistically at the scales relevant to the intended application. That makes the framework useful where precipitation must remain credible across durations and products, including simulation, correction or merging of observations, downscaling, and forecast evaluation. It can show whether the aggregation variability looks plausible, beyond mean and distribution. Moreover, the present analysis is based on a four-year archive and should therefore be interpreted as a characterization of short-record precipitation structure rather than a climatological summary. Even so, this study provides a practical benchmark for comparing precipitation behaviour across different settings.

https://doi.org/10.5194/egusphere-2026-2031
Preprint. Discussion started: 14 April 2026

Appendix A: Point-wise distributional comparison

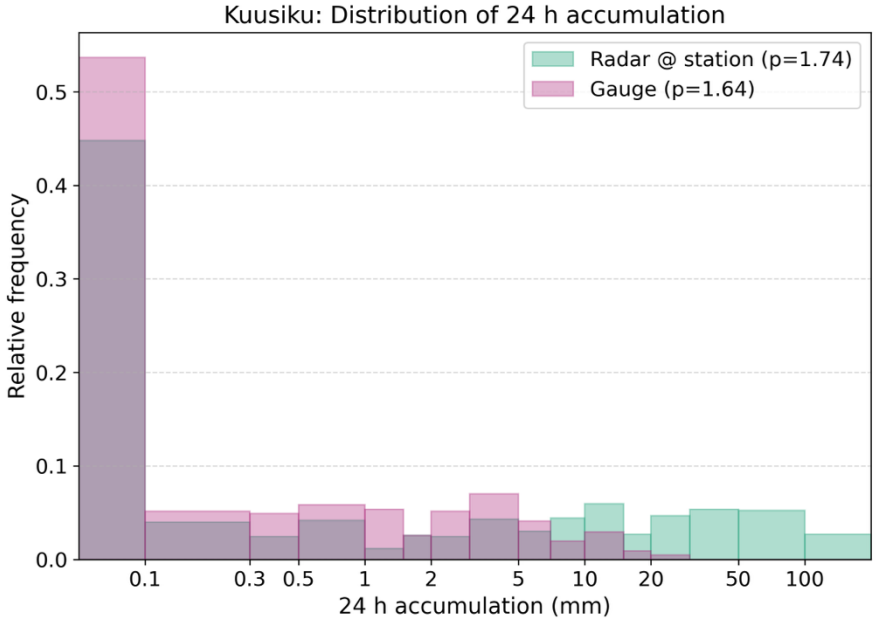

Figure A1: All-year 24 h precipitation distributions at Kuusiku for the radar composite and the corresponding gauge record, on a logarithmic x-axis. The histograms include all totals, with the leftmost bar collecting totals below 0.1 mm, including zeros.

https://doi.org/10.5194/egusphere-2026-2031
Preprint. Discussion started: 14 April 2026

Appendix B: Spatial patterns in inter-season spread

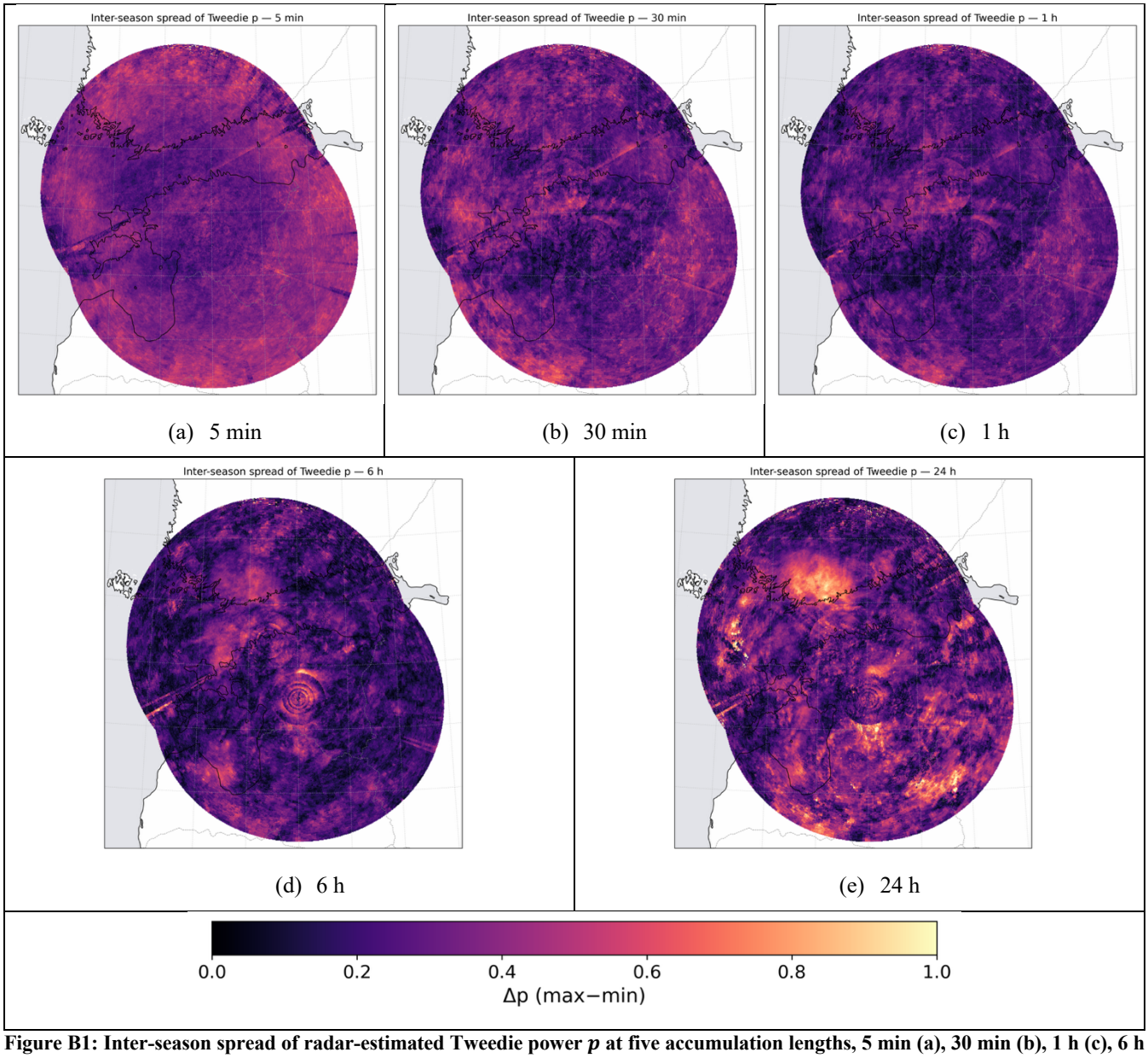

Figure B1: Inter-season spread of radar-estimated Tweedie power *p* at five accumulation lengths, 5 min (a), 30 min (b), 1 h (c), 6 h (d), and 24 h (e).

Appendix C: Radar–gauge agreement maps

Season \ Accumulation	1 h	24 h

https://doi.org/10.5194/egusphere-2026-2031
Preprint. Discussion started: 14 April 2026

ALL	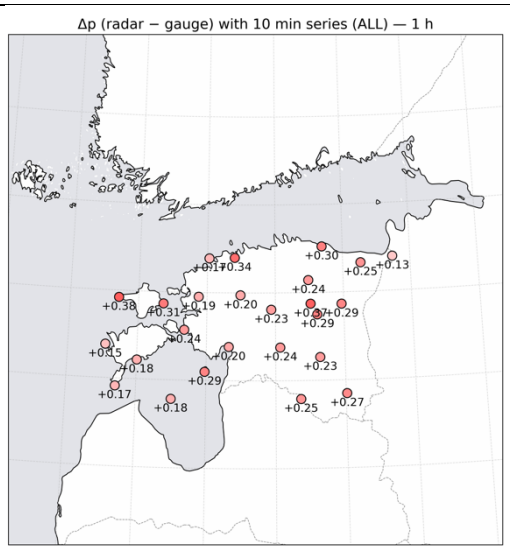 (a)	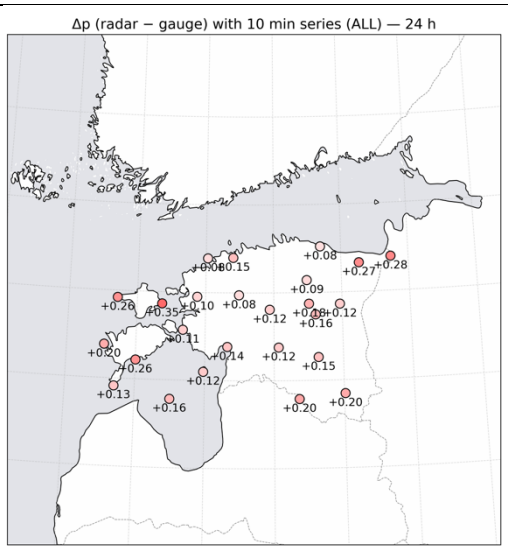 (b)
DJF	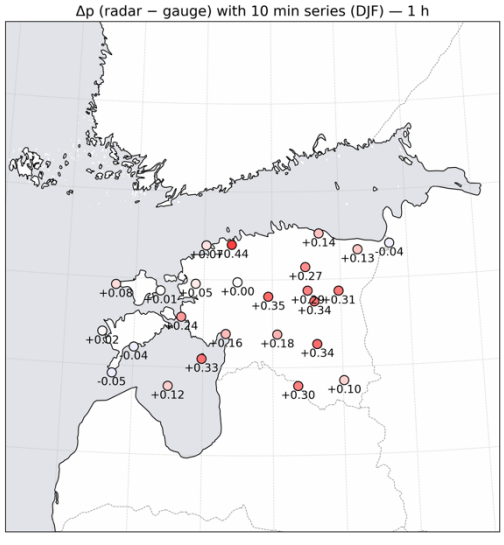 (c)	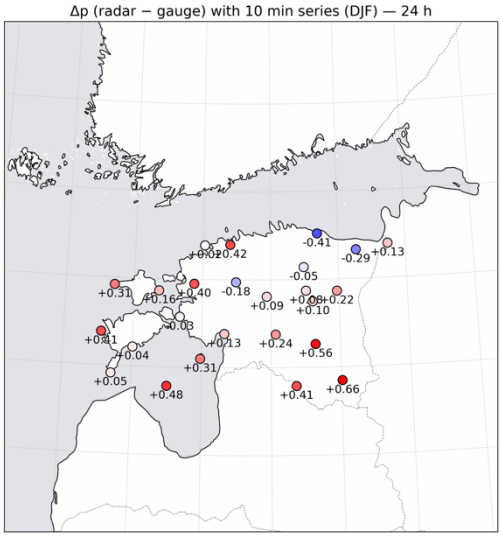 (d)

https://doi.org/10.5194/egusphere-2026-2031
Preprint. Discussion started: 14 April 2026

MAM	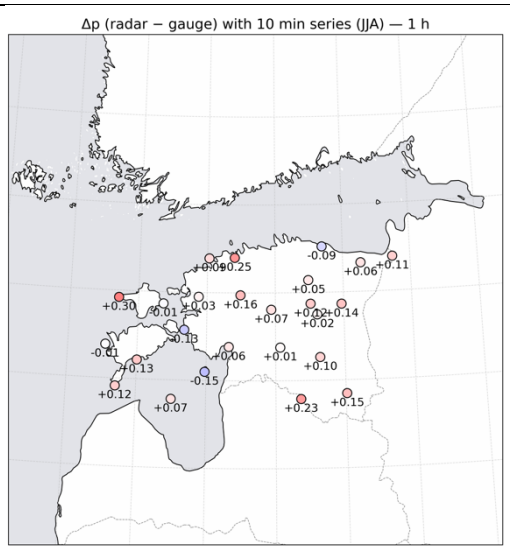 (e)	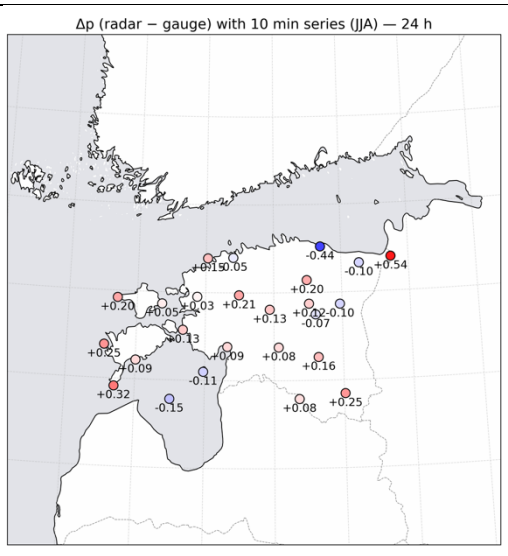 (f)
JJA	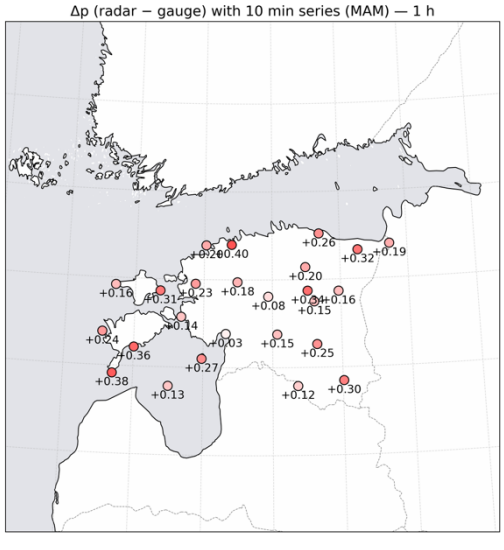 (g)	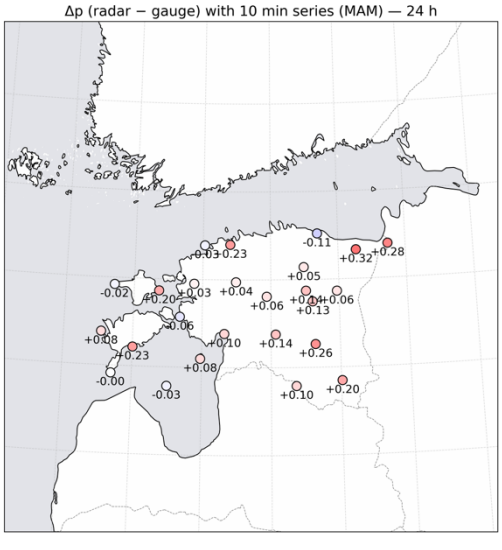 (h)

https://doi.org/10.5194/egusphere-2026-2031
Preprint. Discussion started: 14 April 2026

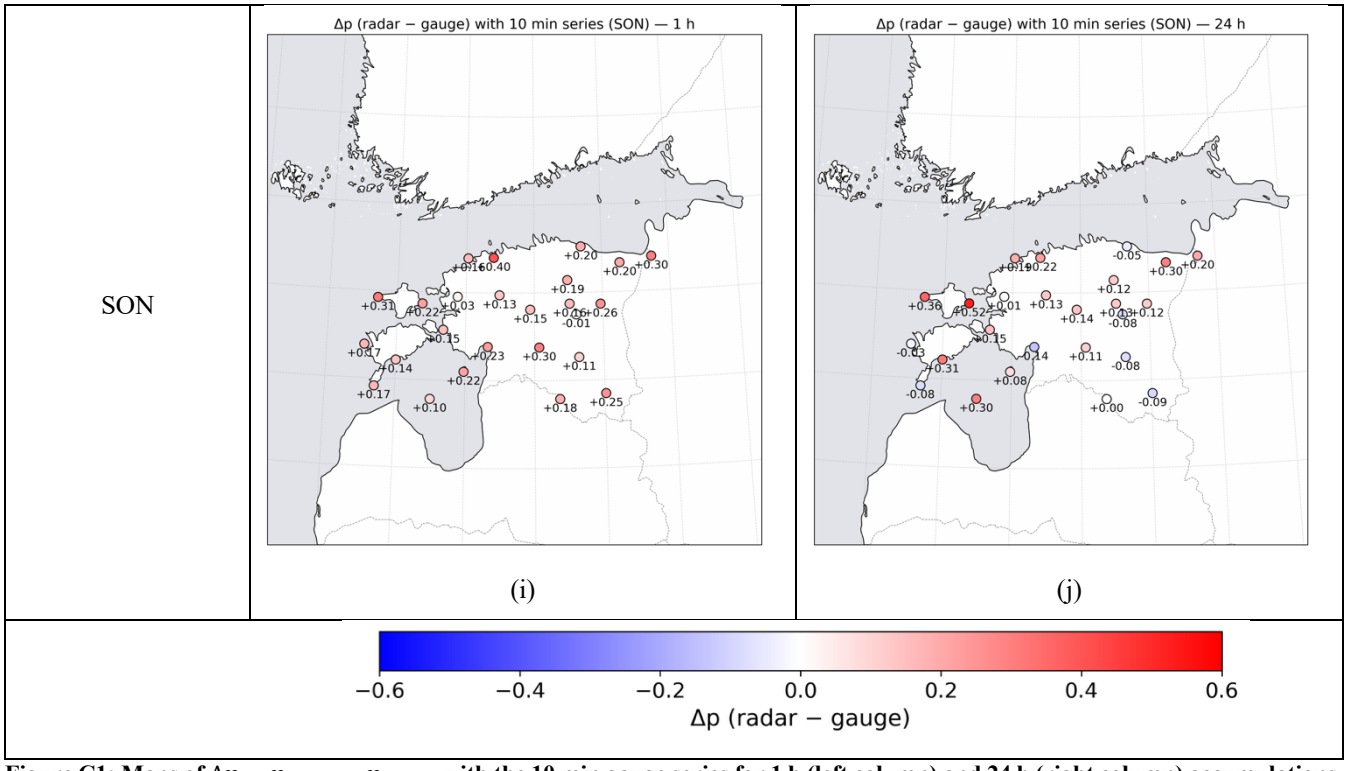

Figure C1: Maps of $\Delta p = p_{radar} - p_{gauge}$ with the 10 min gauge series for 1 h (left column) and 24 h (right column) accumulations. p_{radar} is computed with radar values taken from the grid cells containing the stations. Rows show ALL (a–b), DJF (c–d), MAM (e–f), JJA (g–h), and SON (i–j).

Code and data availability

The weather radar and rain gauge data used in this study are publicly available from the Estonian Environmental Portal through the meteorological radar dataset (https://keskkonnaportaal.ee/et/avaandmed/meteoroloogiliste-radarite-andmestik) and the meteorological monitoring dataset (https://keskkonnaportaal.ee/et/avaandmed/meteoroloogilise-seire-andmestik), respectively. The code used for data processing, computation, and plotting will be made available upon publication.

Author contributions

Conceptualization: YCT. Methodology: YCT. Software: YCT. Formal analysis: YCT. Investigation: YCT. Visualization: YCT. Writing (original draft preparation): YCT. Writing (review and editing): YCT, AM, and SR. Supervision: AM and SR.

Competing interests

The authors declare that they have no conflict of interest.

https://doi.org/10.5194/egusphere-2026-2031
Preprint. Discussion started: 14 April 2026

Acknowledgements

The authors acknowledge the Department of Marine Systems at Tallinn University of Technology for supporting this work. The computations were carried out using the Atlas computing resources of the Department of Marine Systems and the TalTech high-performance computing resources. The authors also acknowledge the Estonian Environmental Agency for making the weather radar and rain gauge data publicly available.

Financial support

This research received no specific grant from any funding agency.

References

Alber, R., Jaagus, J. and Oja, P.: Diurnal cycle of precipitation in Estonia, Estonian Journal of Earth Sciences, 64, https://doi.org/10.3176/earth.2015.36, 2015.

Berne, A. and Krajewski, W.F.: Radar for hydrology: Unfulfilled promise or unrecognized potential?, Advances in Water Resources, 51, 357-366, https://doi.org/10.1016/j.advwatres.2012.05.005, 2013.

Bowler, N.E., Pierce, C.E. and Seed, A.W.: STEPS: A probabilistic precipitation forecasting scheme which merges an extrapolation nowcast with downscaled NWP, Quarterly Journal of the Royal Meteorological Society, 132, 2127-2155, https://doi.org/10.1256/qj.04.100, 2006.

Cambier van Nooten, C., Schreurs, K., Wijnands, J.S., Leijnse, H., Schmeits, M., Whan, K. and Shapovalova, Y.: Improving precipitation nowcasting for high-intensity events using deep generative models with balanced loss and temperature data: A case study in the Netherlands, Artificial Intelligence for the Earth Systems, 2, e230017, https://doi.org/10.1175/AIES-D-23-0017.1, 2023.

Cannon, A.J., Sobie, S.R. and Murdock, T.Q.: Bias correction of GCM precipitation by quantile mapping: how well do methods preserve changes in quantiles and extremes?, Journal of Climate, 28, 6938-6959, https://doi.org/10.1175/JCLI-D-14-00754.1, 2015.

Chapman, T.: Stochastic modelling of daily rainfall: the impact of adjoining wet days on the distribution of rainfall amounts, Environmental Modelling & Software, 13, 317-324, https://doi.org/10.1016/S1364-8152(98)00036-X, 1998.

Chin, E. H.: Modeling daily precipitation occurrence process with Markov chain, Water Resources Research, 13, 949-956, https://doi.org/10.1029/WR013i006p00949, 1977.

Cremonini, R., Voormansik, T., Post, P. and Moisseev, D.: Estimation of extreme precipitation events in Estonia and Italy using dual-polarization weather radar quantitative precipitation estimations, Atmospheric Measurement Techniques, 16, 2943-2956, https://doi.org/10.5194/amt-16-2943-2023, 2023.

https://doi.org/10.5194/egusphere-2026-2031
Preprint. Discussion started: 14 April 2026

Ficchì, A., Perrin, C. and Andréassian, V.: Impact of temporal resolution of inputs on hydrological model performance: An analysis based on 2400 flood events, Journal of Hydrology, 538, 454-470, https://doi.org/10.1016/j.jhydrol.2016.04.016, 2016.

Gabriel, K. R. and Neumann, J.: A Markov chain model for daily rainfall occurrence at Tel Aviv, Quarterly Journal of the Royal Meteorological Society, 88, 90-95, https://doi.org/10.1002/qj.49708837511, 1962.

Germann, U. and Zawadzki, I.: Scale-dependence of the predictability of precipitation from continental radar images. Part I: Description of the methodology, Monthly Weather Review, 130, 2859-2873, https://doi.org/10.1175/1520-0493(2002)130%3C2859:SDOTPO%3E2.0.CO;2, 2002.

Goudenhoofdt, E. and Delobbe, L.: Evaluation of radar-gauge merging methods for quantitative precipitation estimates, Hydrology and Earth System Sciences, 13, 195-203, https://doi.org/10.5194/hess-13-195-2009, 2009.

Hasan, M.M., Croke, B.F. and Karim, F.: Spatial and seasonal variations and inter-relationship in fitted model parameters for rainfall totals across Australia at various timescales, Climate, 7, 4, https://doi.org/10.3390/cli7010004, 2019.

Hasan, M. M. and Dunn, P. K.: A simple Poisson–gamma model for modelling rainfall occurrence and amount simultaneously, Agricultural and Forest Meteorology, 150, 1319-1330, https://doi.org/10.1016/j.agrformet.2010.06.002, 2010.

Huang, Y., Bárdossy, A. and Zhang, K.: Sensitivity of hydrological models to temporal and spatial resolutions of rainfall data, Hydrology and Earth System Sciences, 23, 2647-2663, https://doi.org/10.5194/hess-23-2647-2019, 2019.

Hunt, K. M. R.: Stop using root-mean-square error as a precipitation target!, arXiv preprint arXiv:2509.08369, https://doi.org/10.48550/arXiv.2509.08369, 2025.

Imhoff, R.O., Brauer, C.C., Overeem, A., Weerts, A.H. and Uijlenhoet, R.: Spatial and temporal evaluation of radar rainfall nowcasting techniques on 1,533 events, Water Resources Research, 56, e2019WR026723, https://doi.org/10.1029/2019WR026723, 2020.

Imhoff, R.O., Brauer, C.C., van Heeringen, K.J., Uijlenhoet, R. and Weerts, A.H.: Large-sample evaluation of radar rainfall nowcasting for flood early warning, Water Resources Research, 58, e2021WR031591, https://doi.org/10.1029/2021WR031591, 2022.

Jaagus, J., Briede, A., Rimkus, E. and Remm, K.: Precipitation pattern in the Baltic countries under the influence of large-scale atmospheric circulation and local landscape factors, International Journal of Climatology, 30, 705-720, https://doi.org/10.1002/joc.1929, 2010.

Jaagus, J., Post, P. and Tomingas, O.: Changes in storminess on the western coast of Estonia in relation to large-scale atmospheric circulation, Climate Research, 36, 29-40, https://doi.org/10.3354/cr00725, 2008.

Kossieris, P., Makropoulos, C., Onof, C. and Koutsoyiannis, D.: A rainfall disaggregation scheme for sub-hourly time scales: Coupling a Bartlett-Lewis based model with adjusting procedures, Journal of Hydrology, 556, 980-992, https://doi.org/10.1016/j.jhydrol.2016.07.015, 2018.

Krajewski, W.F. and Smith, J.A.: Radar hydrology: Rainfall estimation, Advances in Water Resources, 25, 1387-1394, https://doi.org/10.1016/S0309-1708(02)00062-3, 2002.

https://doi.org/10.5194/egusphere-2026-2031
Preprint. Discussion started: 14 April 2026

Langousis, A. and Veneziano, D.: Intensity-duration-frequency curves from scaling representations of rainfall, Water Resources Research, 43, https://doi.org/10.1029/2006WR005245, 2007.

Mändla, K., Enno, S.E. and Sepp, M.: Thunderstorms caused by southern cyclones in Estonia, Estonian Journal of Earth Sciences, 63, https://doi.org/10.3176/earth.2014.10, 2014.

Mändla, K., Sepp, M. and Jaagus, J.: Climatology of cyclones with a southern origin, and their influence on air temperature and precipitation in Estonia, Boreal Environment Research, 17, https://doi.org/10.60910/by2q-4znc, 2012.

Maraun, D.: Bias correction, quantile mapping, and downscaling: Revisiting the inflation issue. Journal of Climate, 26, 2137-2143, https://doi.org/10.1175/JCLI-D-12-00821.1, 2013.

Maraun, D., Wetterhall, F., Ireson, A.M., Chandler, R.E., Kendon, E.J., Widmann, M., Brienen, S., Rust, H.W., Sauter, T., Themeßl, M. and Venema, V.K.: Precipitation downscaling under climate change: Recent developments to bridge the gap between dynamical models and the end user, Reviews of geophysics, 48, https://doi.org/10.1029/2009RG000314, 2010.

Marra, F. and Morin, E.: Use of radar QPE for the derivation of Intensity–Duration–Frequency curves in a range of climatic regimes, Journal of Hydrology, 531, 427-440, https://doi.org/10.1016/j.jhydrol.2015.08.064, 2015.

Martinez-Villalobos, C. and Neelin, J. D.: Why Do Precipitation Intensities Tend to Follow Gamma Distributions?, Journal of the Atmospheric Sciences, 76, 3611-3631, https://doi.org/10.1175/JAS-D-18-0343.1, 2019.

Mazon, J., Niemelä, S., Pino, D., Savijärvi, H. and Vihma, T.: Snow bands over the Gulf of Finland in wintertime, Tellus A: Dynamic Meteorology and Oceanography, 67, https://doi.org/10.3402/tellusa.v67.25102, 2015.

Menabde, M. and Sivapalan, M.: Modeling of rainfall time series and extremes using bounded random cascades and levy-stable distributions, Water Resources Research, 36, 3293-3300, https://doi.org/10.1029/2000WR900197, 2000.

Ochoa-Rodriguez, S., Wang, L.P., Willems, P. and Onof, C.: A review of radar-rain gauge data merging methods and their potential for urban hydrological applications, Water Resources Research, 55, 6356-6391, https://doi.org/10.1029/2018WR023332, 2019.

Olsson, J., Dyrrdal, A.V., Médus, E., Södling, J., Aņiskeviča, S., Arnbjerg-Nielsen, K., Førland, E., Mačiulytė, V., Mäkelä, A., Post, P. and Thorndahl, S.L.: Sub-daily rainfall extremes in the Nordic–Baltic region, Hydrology Research, 53, 807-824, https://doi.org/10.2166/nh.2022.119, 2022.

Olsson, T., Luomaranta, A., Jylhä, K., Jeworrek, J., Perttula, T., Dieterich, C., Wu, L., Rutgersson, A. and Mäkelä, A.: Statistics of sea-effect snowfall along the Finnish coastline based on regional climate model data, Advances in Science and Research, 17, https://doi.org/10.5194/asr-17-87-2020, 2020.

Paschalis, A., Molnar, P., Fatichi, S. and Burlando, P.: On temporal stochastic modeling of precipitation, nesting models across scales, Advances in Water Resources, 63, 152-166, https://doi.org/10.1016/j.advwatres.2013.11.006, 2014.

Post, P., Truija, V. and Tuulik, J.: Circulation weather types and their influence on temperature and precipitation in Estonia, Boreal Environment Research, 7, 281-289, https://doi.org/10.60910/dp0h-gm6x, 2002.

https://doi.org/10.5194/egusphere-2026-2031
Preprint. Discussion started: 14 April 2026

Prudden, R., Adams, S., Kangin, D., Robinson, N., Ravuri, S., Mohamed, S. and Arribas, A.: A review of radar-based nowcasting of precipitation and applicable machine learning techniques, arXiv preprint arXiv:2005.04988, https://doi.org/10.48550/arXiv.2005.04988, 2020.

Rajagopalan, B., Lall, U. and Tarboton, D. G.: Nonhomogeneous Markov Model for Daily Precipitation, Journal of Hydrological Engineering, 1, 33-40, https://doi.org/10.1061/(ASCE)1084-0699(1996)1:1(33), 1996.

Ravuri, S., Lenc, K., Willson, M., Kangin, D., Lam, R., Mirowski, P., Fitzsimons, M., Athanassiadou, M., Kashem, S., Madge, S. and Prudden, R.: Skilful precipitation nowcasting using deep generative models of radar, Nature, 597, 672-677, https://doi.org/10.1038/s41586-021-03854-z, 2021.

Remm, K., Jaagus, J., Briede, A., Rimkus, E. and Kelviste, T.: Interpolative mapping of mean precipitation in the Baltic countries by using landscape characteristics, Estonian Journal of Earth Sciences, 60, 172, https://doi.org/10.3176/earth.2011.3.05, 2011.

Richardson, C.W.: Stochastic simulation of daily precipitation, temperature, and solar radiation, Water resources research, 17, 182-190, https://doi.org/10.1029/WR017i001p00182, 1981.

Röthlisberger, M., Scherrer, B., de Vries, A.J. and Portmann, R.: The role of cyclones and PV cutoffs for the occurrence of unusually long wet spells in Europe, Weather and Climate Dynamics Discussions, 2022, 1-31, https://doi.org/10.5194/wcd-3-733-2022, 2022.

Rydén, J.: Statistical analysis of monthly precipitation in Sweden using the Tweedie distribution, Theoretical and Applied Climatology, 156, 512, https://doi.org/10.1007/s00704-025-05792-6, 2025.

Sansom, J. and Thompson, P.: Fitting Hidden Semi-Markov Models to Breakpoint Rainfall Data, Journal of Applied Probability, 38, 142-157, https://doi.org/10.1239/jap/1085496598, 2001.

Savijärvi, H.I.: Cold air outbreaks over high-latitude sea gulfs, Tellus A: Dynamic Meteorology and Oceanography, 64, https://doi.org/10.3402/tellusa.v64i0.12244, 2012.

Segond, M.L., Onof, C. and Wheater, H.S.: Spatial–temporal disaggregation of daily rainfall from a generalized linear model, Journal of Hydrology, 331, 674-689, https://doi.org/10.1016/j.jhydrol.2006.06.019, 2006.

Seo, B.C., Krajewski, W.F., Kruger, A., Domaszczynski, P., Smith, J.A. and Steiner, M.: Radar-rainfall estimation algorithms of Hydro-NEXRAD, Journal of Hydroinformatics, 13, 277-291, https://doi.org/10.2166/hydro.2010.003, 2011.

Singh, S., Maljutenko, I. and Uiboupin, R.: Sea ice in the Baltic Sea during 1993/94–2020/21 ice seasons from satellite observations and model reanalysis, The Cryosphere, 19, https://doi.org/10.5194/tc-19-4741-2025, 2025.

Small, M. J. and Morgan, D. J.: The Relationship Between a Continuous-Time Renewal Model and a Discrete Markov Chain Model of Precipitation Occurrence, Water Resources Research, 22, 1422-1430, https://doi.org/10.1029/WR022i010p01422, 1986.

Sokol, Z., Szturc, J., Orellana-Alvear, J., Popova, J., Jurczyk, A. and Célleri, R.: The role of weather radar in rainfall estimation and its application in meteorological and hydrological modelling—A review, Remote Sensing, 13, 351, https://doi.org/10.3390/rs13030351, 2021.

https://doi.org/10.5194/egusphere-2026-2031
Preprint. Discussion started: 14 April 2026

Svensson, C., Hannaford, J. and Prosdocimi, I.: Statistical distributions for monthly aggregations of precipitation and streamflow in drought indicator applications, Water Resources Research, 53, 999-1018, https://doi.org/10.1002/2016WR019276, 2017.

Tabari, H., Paz, S.M., Buekenhout, D. and Willems, P.: Comparison of statistical downscaling methods for climate change impact analysis on precipitation-driven drought, Hydrology and Earth System Sciences, 25, 3493-3517, https://doi.org/10.5194/hess-25-3493-2021, 2021.

Tabary, P.: The new French operational radar rainfall product. Part I: Methodology, Weather and Forecasting, 22, 393-408, https://doi.org/10.1175/WAF1004.1, 2007.

Virman, M., Olsson, T., Lind, P. and Jylhä, K.: Sea-effect snowfall in the Baltic Sea area in 1998–2018 derived from convection-permitting climate model data, EGUsphere, 2025, https://doi.org/10.5194/egusphere-2025-3663, 2025.

Voormansik, T., Cremonini, R., Post, P. and Moisseev, D.: Evaluation of the dual-polarization weather radar quantitative precipitation estimation using long-term datasets, Hydrology and Earth System Sciences, 25, 1245-1258, https://doi.org/10.5194/hess-25-1245-2021, 2021.

Voormansik, T., Müürsepp, T. and Post, P.: Climatology of convective storms in Estonia from radar data and severe convective environments, Remote Sensing, 13, https://doi.org/10.3390/rs13112178, 2021.

Wheater, H.S., Chandler, R.E., Onof, C.J., Isham, V.S., Bellone, E., Yang, C., Lekkas, D., Lourmas, G. and Segond, M.L.: Spatial-temporal rainfall modelling for flood risk estimation, Stochastic Environmental Research and Risk Assessment, 19, 403-416, https://doi.org/10.1007/s00477-005-0011-8, 2005.

Wilks, D.S.: Multisite downscaling of daily precipitation with a stochastic weather generator, Climate research, 11, 125-136, https://doi.org/10.3354/cr011125, 1999.